VII Brazilian Symposium on Rock Mechanics – SBMR 2016
Rock Mechanics and Rock Engineering for Innovation and Development
ISRM Specialized Conference 19-22 October, Belo Horizonte, Minas Gerais, Brazil

Numerical modeling of fracture containment in multi-layered formations using a cohesive zone model

Renato Gutierrez Escobar
TECGRAF PUC-RIO, Rio de Janeiro, Brasil, renatogu@tecgraf.puc-rio.br

Eleazar Cristian Mejia Sanchez
TECGRAF PUC-RIO, Rio de Janeiro, Brasil, crisms@tecgraf.puc-rio.br

Deane de Mesquita Roehl
TECGRAF PUC-RIO, Rio de Janeiro, Brasil, deane@tecgraf.puc-rio.br

Celso Romanel
PUC-RIO, Rio de Janeiro, Brasil, romanel@puc-rio.br

SUMMARY: One of the challenges of the hydraulic fracturing operation is the determination of the fluid-driven vertical fracture extent. In cases such as cuttings re-injection and CO2 sequestration fractures must be contained mainly to the pay zone since fracture breakout into overlaying or underlying formations with water-bearing zone can lead to irreparable water damage to the formation, Cormack et. al, (1983). Numerical modelling of hydraulic fracturing can reduce uncertainties in the reservoir integrity. Parametric studies help define critical conditions and predict the most favorable scenarios. In this work, a fully coupled cohesive fracture model is used to simulate hydraulic fracturing processes considering the propagation of a vertical planar fluid-driven fracture for a transient analyses. This paper is focused on the pressure required for crack extension and on the resulting fracture geometry considering the injection procedure as a concentrated fluid flow. The influence of the vertical variation in tectonic stress, the elastic stiffness and the critical stress intensity factor on the fracture behavior are investigated. A finite element model with coupled cohesive elements was used for the simulation of rock fracture. Symmetrical (no vertical variation in tectonic stress) and asymmetrical (vertical variation in tectonic stress) tri-layered formations were studied and compared to the analytical solutions proposed by Simonson (1977) and Fung (1987). According to these results, the predicted pore pressure for crack propagation exhibits good agreement with the analytical solutions. As expected, the mechanism of fracture containment has proven to be the vertical variation in tectonic stresses and critical stress intensity factor. On the other hand, the contrasts in the elastic stiffness do not act as effective barriers to vertical fracture propagation.

KEYWORDS: Hydraulic Fracturing, Coupled Cohesive Element, Petroleum Geomechanics, Fracture Mechanics, Fracture Containment, Fracture Propagation

1 INTRODUCTION

Massive hydraulic fractures are playing a major role in the recovery of reserves of gas tied up in the tight gas sands of the deep basin. One of the major problems in designing fractures in such formations is the uncertain vertical extent of these fractures.

The hydraulic fracture containment is the main issue to be investigated. It is essential to ensure the fractures are contained within the pay zone without breakout into overlying or underlying formations in order to avoid serious consequences on the effectiveness of the operation. On the other hand, the study of the containment of vertical hydraulic fractures is performed to understand the parameters and conditions that will limit the fracture height, control its direction and determine its critical fracture pressure.

In this paper, the analytical solutions for computing vertical fracture extent in multilayered formations and its numerical results are compared. The numerical solution was carried out using the finite element method with a cohesive zone model. In addition, the influence of the most important parameters involved in fracture propagation has also been studied.

2 ANALITYCAL SOLUTIONS

2.1 Simonson's Solution (1978)

Based on linear elastic fracture mechanics, Simonson developed an analytical solution of the vertical fracture extent in homogeneous reservoirs with symmetrical in-situ stress between layers, as described in Figure 1.

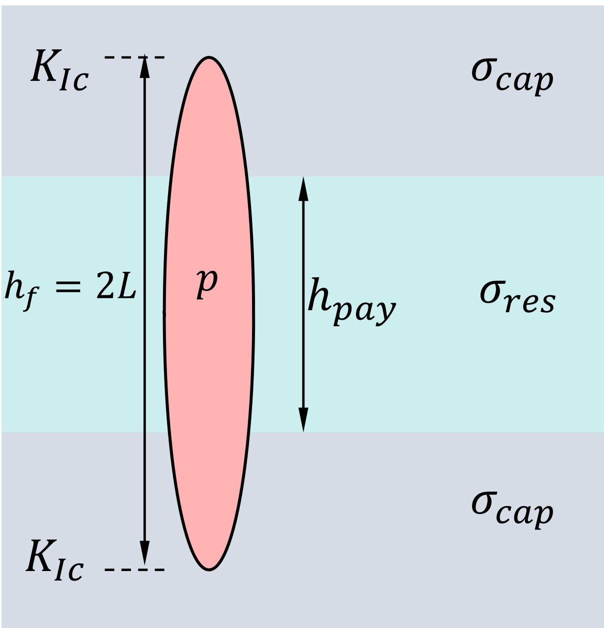

Figure 1. Simonson's analytical model

According to Simonson's solution the internal fracture pressure P required for fracture penetration into the adjacent zones is given by the following equation:

$$P = \sigma_{res} + \frac{K_{1C}}{\sqrt{\pi L}} + \frac{2(\sigma_{cap} - \sigma_{res})}{\pi} \cos^{-1}\left(\frac{h_{pay}}{2L}\right) \quad (1)$$

where K_{Ic} is the stress intensity factor, $h_f = 2L$ is the fracture height, σ_{res} is the horizontal stress in the reservoir, σ_{cap} is the horizontal stress of the barrier layers, and h_{pay} is the height of the reservoir layer.

2.2 Fung's Solution (1987)

Based on the work proposed by Simonson, Fung developed a more general solution for computing vertical fracture extent in multilayer reservoirs with an arbitrary in-situ horizontal stress distribution. The schematic representation of the non-symmetric multilayer reservoir is depicted in Figure 2.

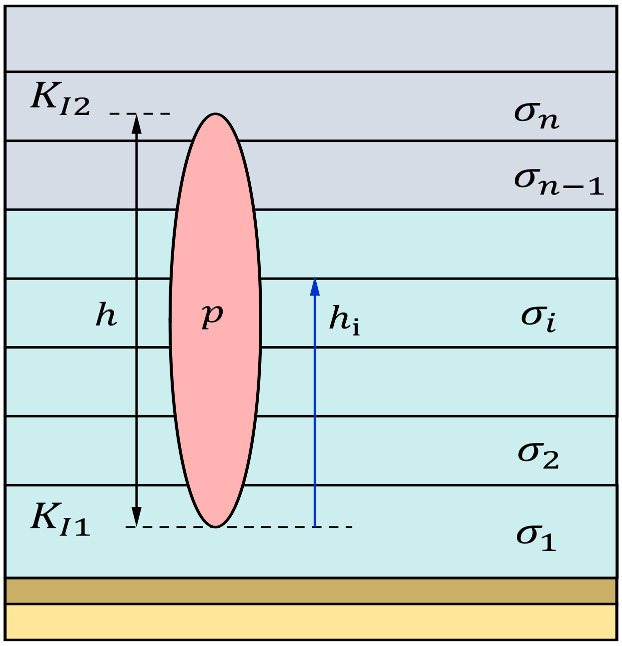

Figure 2. Fung's analytical model

Considering plane stress conditions the stress intensity factors at the lower and upper crack tips K_{I1} and K_{I2}, respectively, can be defined based on the internal fracture pressure P and the in-situ horizontal stresses σ_i as:

$$K_{Im} = \sqrt{\frac{h}{2\pi}}.\left\{(P - \sigma_n)\pi + \sum_{i=1}^{n}(\sigma_{i+1} - \sigma_i).\right.$$
$$\left.\left[2\sin^{-1}\sqrt{\frac{h_i}{h}} - (-1^m)\sqrt{1 - \left(\frac{2h_i - h}{h}\right)^2}\right]\right\} \quad (2)$$

Where m is 1 or 2 for the lower and upper tips, respectively, h is the total fracture height and h_i is the distance from the lower crack tip to the top of layer i.

For a fracture in equilibrium, the stress intensity factors equals the critical values ($K_I = K_{Ic}$) for the fractured layers, Cormack (1983). From equation 2, the difference between upper and lower stress intensity factors at equilibrium can be computed as:

$$K_{Ic1} - K_{Ic2} = \sqrt{\frac{h}{2\pi}} \sum_{i=1}^{n} \left\{ (\sigma_{i+1} - \sigma_i) . \sqrt{1 - \left(\frac{2h_i - h}{h}\right)^2} \right\} \quad (3)$$

Based on equation 3, the total fracture height h can be obtained using the bisection iteration for a specified lower crack tip location. Then, the internal fracture pressure P is obtained substituting the total fracture height into equation 2. Thus, the lower fracture tip is moved slightly in the formation and the new upper fracture tip is obtained. In this manner, the internal fracture pressure is obtained for each total fracture height, generating a complete fracture map. The described semi analytical procedure was programmed in GNU Octave.

3 NUMERICAL MODELLING

In this section, the geometry of synthetic models, the simulation steps, and the initial and boundary conditions are described.

3.1 Simulation steps

For each case studied, the same simulation steps were applied. The first step called Geostatic step determines the geostatic equilibrium between the initial loads (stresses and pore pressure) and the boundary conditions. The initial loads can be applied programming subroutines such as Sigini, Uporep and Disp (Abaqus, 2014). In the second step defined as a consolidation analysis, the fluid injection is performed as a prescribed flow rate injection of a Newtonian fluid in order to be compare with its analytical solutions (Geertsma, 1979; Khristianovic, 1955 and Nordgren, 1972).

3.2 Synthetic models

In order to compare the analytical and the numerical results, synthetic models are constructed. These synthetic models are discretized by a two-dimensional quadrilateral element CPE4, without a pore pressure degree of freedom to represent the adjacent porous media, and cohesive elements COH2D4P, with a pore pressure degree of freedom to model the fracture propagation (Cheng, 2009 and Shen, 2012). The geometry of the synthetic models is described in Figures 3 and 4.

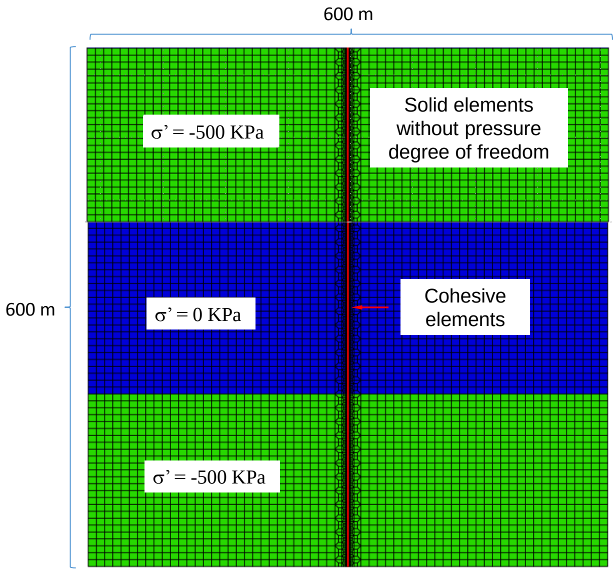

Figure 3. Numerical model with symmetrical stress constrast

Figure 3 exhibits the numerical model with a symmetrical in-situ stress contrast (no vertical variation in tectonic stresses) used to be compared with Simonson's analytical solution.

On the other hand, Figure 4 shows an asymmetrical in-situ stress contrast to be compared with the analytical solution given by Fung's model.

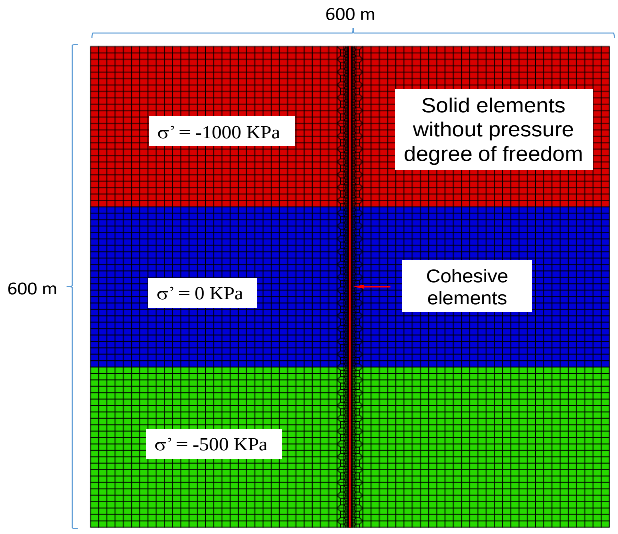

Figure 4. Numerical model with asymmetrical stress constrast

The material parameters used for all simulations are the same as those used by Zielonka in his work (Zielonka, et.al. 2014). Those parameters are summarized in Table 1.

Table 1. Material properties

Properties	Value
Intact rock	
Young Modulus (Gpa)	17
Poisson Ratio	0.2
Porosity	0.2
Hydraulic Conductivity (m/s)	9.80E-09
Fracturing Fluid	
Specific Weight (kN/m3)	9.8
Viscosity (kPa.s)	1.00E-07
Fracture	
Cohesive Energy (Pa.m)	120
Critical Stress Intensity Factor (MPa.$\sqrt{m}$)	1.46
Rock Strenght (Mpa)	1.25

In order to study the influence of in-situ stresses and pore pressure contrast on the fracture extent in adjacent layers, different cases of initial conditions are simulated. The initial stresses and pore pressure for each case are listed in Table 2.

Table 2. Initial conditions for the studied cases

Layers	Units	Case 1	Case 2	Case 3
Layer 1	σ_{ef} [kPa]	3000	4000	2000
	P_0 [kPa]	2000	2000	2000
Layer 2	σ_{ef} [kPa]]	1000	1000	1000
	P_0 [kPa]	1000	1000	1000
Layer 3	σ_{ef} [kPa]	2000	2000	4000
	P_0 [kPa]	3000	3000	3000

4 RESULTS AND DISCUSSIONS

4.1 Numerical solution vs Simonson solution

The numerical results for symmetrical layers and Simonson's solutions are almost identical for the first 100 meters (propagation under the reservoir layer). Hereafter, the fracture penetrates into the adjacent layers where the in-situ horizontal stresses are greater than in the reservoir layer, causing an increase of the internal fracture pressure (h = 100 m to 150 m) required for fracture propagation. However, the numerical results and the analytical solution for this region show a small difference, as in Figure 5.

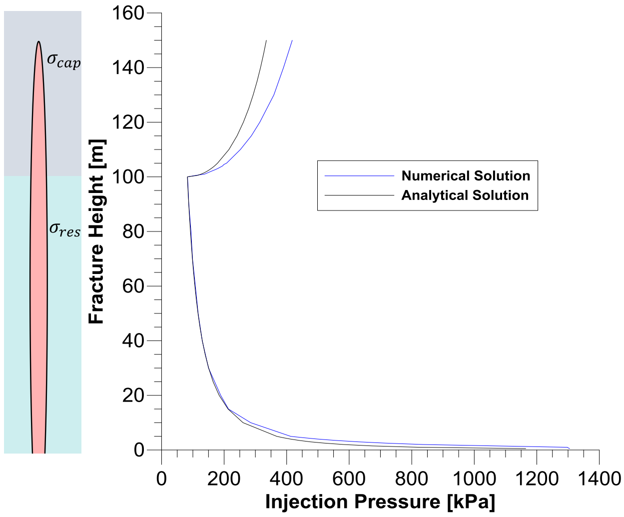

Figure 5. Comparison between Simonson and numerical model

This discrepancy occurs because the analytical solution is based on the linear elastic fracture mechanics while the numerical model considers a coupled hydro-mechanical solution.

4.2 Numerical solution vs Fung solution

Figure 6 shows the fracture map for a trilayered formation with nonsymmetrical in-situ stress distribution as detailed in Figure 4 (-500 kPa at the lower layer and -1000 kPa at the upper layer). We can observe that the fracture pressure required to extend the fracture into the bounding layers is shown as a function of the fracture height.

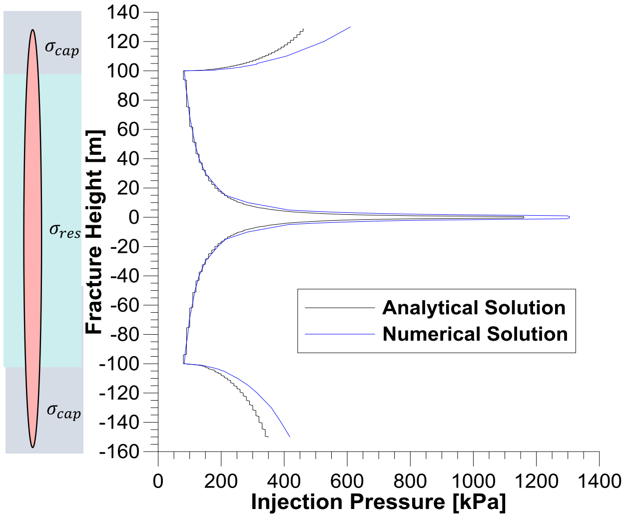

Figure 6. Comparison between Fung's solution and the numerical model

The numerical results obtained for fracture propagation at the pay layer agrees very closely with the obtained by Fung's analytical procedure (δ = 0 to 100 m). As expected, the computed internal fracture pressure P increases according to the distance of penetration into the bounding layer. However, the numerical results for fracture propagation in the upper layer and lower layer differ from those obtained by Fung's analytical solution. In addition, the fracture penetrates farther into the lower layer because this layer has lower in-situ stresses in comparison with the upper layer, as shown in Figure 6.

Once again, the slight differences between the analytical and numerical results are justified because the analytical solution is based on the linear elastic fracture mechanics while the numerical model considers a coupled hydro-mechanical solution.

4.3 Effect of in-situ stress distribution and pore pressure

In geotechnical applications, it is well-known that the multilayered formations can exhibit an in-situ tectonic stress and pore pressure distribution. In order to study the effect of the initial pore pressure and the in-situ tectonic stress distribution on the behavior of fracture propagation, three different cases are simulated, as detailed in Table 2. Then, for provided initial pore pressure and in-situ tectonic stresses, the fracture extension pressure can be computed using Fung's approach.

Figure 7 shows the crack length vs the crack opening and crack length vs injection pressure, computed with the numerical procedure, for case 1, as detailed in Table 2.

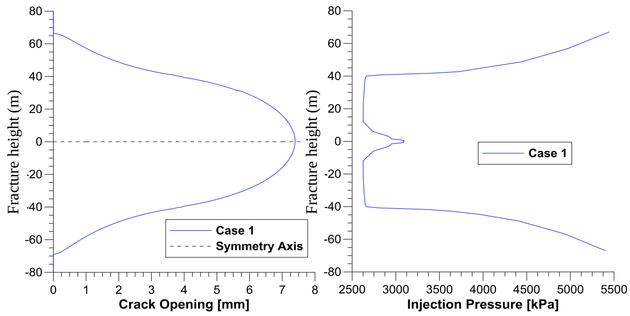

Figure 7. Symmetrical fracture propagation generated by pore pressure influence

Although the initial load conditions (pore pressure and in-situ tectonic stresses) are very different from one layer to the other, the fracture extends symmetrically into both directions (upper and lower layer) as depicted in Figure 7. In this case, the upper and lower layers are undergoing the same total stress ($\sigma_T = 5000$ kPa) causing a symmetric distribution of the injection pressure when the fracture penetrates into the adjacent layers (further 40m and -40m).

Case 2 assumes the total stress at the upper layer $\sigma_{Tup} = 6000$ kPa is greater than at the lower layer $\sigma_{Tlw} = 5000$ kPa. According to the numerical results, the fracture penetrates further into the lower layer with a slightly smaller injection pressure than the one required for penetration into the upper layer, as shown in Figure 8.

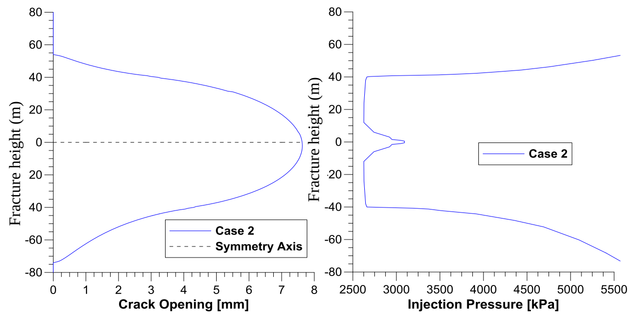

Figure 8. Asymmetrical fracture propagation generated by pore pressure influence

In case 3, the total stress at the lower layer $\sigma_{Tlw} = 7000$ kPa is greater than at the upper layer $\sigma_{Tup} = 4000$ kPa. As expected, the fracture penetrates further into the upper layer and with a smaller injection pressure (further 40m), as shown in Figure 9.

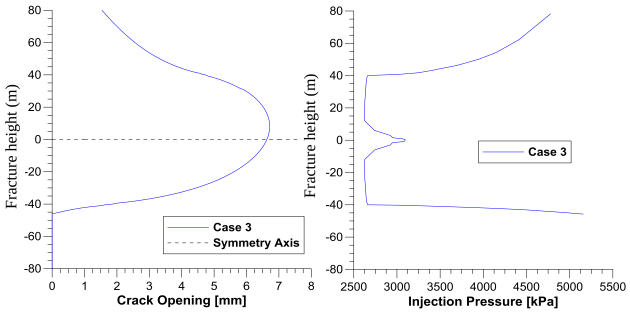

Figure 9. Asymmetrical fracture propagation generated by porepressure influence

In addition, the total stress contrast $\Delta\sigma_T = |\sigma_{Tup} - \sigma_{Tlw}|$ between the lower and upper layer determines the facility to extend the fracture towards the layer with the lowest total stress. For instance, fracture penetration into the upper layer in case 3 is higher than the penetration reported in case 2 into the lower layer, because the total stress contrast reported in case 3 is higher.

4.4 Parametric study

4.4.1 Young's Modulus effects

As Young's modulus is increased, the rock becomes stiffer. That is why the pressure profile along the fracture increases in order to deform the medium and the fracture tends to be longer than wide, figures 17 and 18.

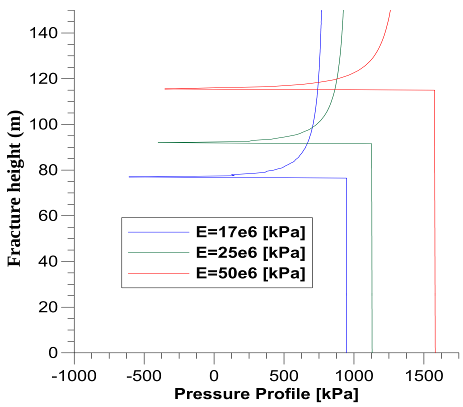

Figure 17. Pressure profile along the fracture

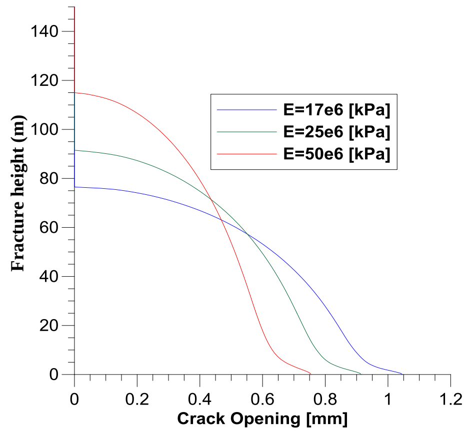

Figure 18. Fracture geometry

4.4.2 Critical stress intensity factor effects

The greater the critical stress intensity factor, the higher the injection pressure required to propagate the fracture. On the other hand, high stress intensity factors produce shorter and wider fractures, as shown in figures 19 and 20.

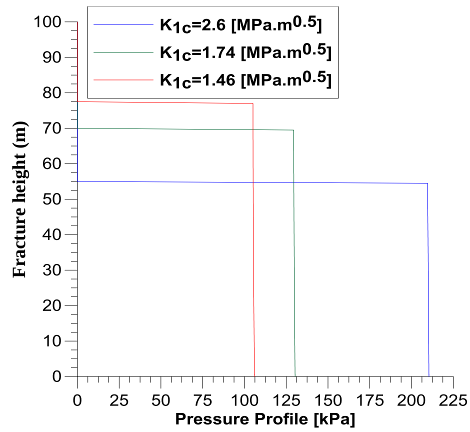

Figure 19. Pressure profile along the fracture

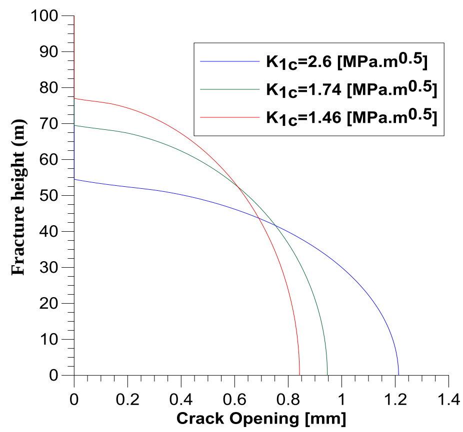

Figure 20. Fracture geometry

CONCLUSIONS

Analytical models of fracture propagation in adjacent layers with symmetrical horizontal stress contrast (Simonson 1978) and asymmetrical contrast (Fung 1987) were compared to numerical models, having a reasonable agreement throughout the fracture propagation in the reservoir. When fracture penetrates the adjacent layers considering the stress contrast, differences on the results are observed, justified on the simplicity of the analytical models based on the linear elastic fracture mechanics in comparison to the coupled hydro-mechanical finite element solution.

Fractures are constrained in transient analysis for the pore pressure excess generated in the deformed porous media, as the cohesive elements becomes wider by the injection process.

Elastic stiffness contrast was concluded not to be a significant containment mechanism, unlike the critical stress intensity factor and the horizontal stress contrast which constraint the fracture propagation effectively.

ACKNOWLEDGEMENTS

This work was supported by the Pontifical Catholic University of Rio de Janeiro, Brazil.,

REFERENCES

Abaqus User's Manual. (2014). *Dassault Systèmes Simulia Corp.*, Providence, RI. 2014.

Cheng, Z., Bunger, A.P., Zhang, X., Jeffrey, R. G. (2009). Cohesive zone finite element-based modeling of hydraulic fractures, *Acta Mechanica Solida Sinica*, Vol. 22, No. 5.

Cormack, D.E, Fung, R.L., Vijayakumar, S. (1983) Vertical fracture containment during massive hydraulic fracturing. *The 34th annual technical meeting of the petroleum society of cim*, Banff, Canada.

Economides, M. J., And Nolte, K. N. (2000). *Reservoir stimulation*, Third Edition, Jhon Wiley & Sons Ltd.

Fung, R. L., Vijayakumar, S., Cormack, D. E. (1987). Calculation of Vertical Fracture Containment in Layered Formations, *Society of petroleum engineers journal.*

Geertsma, J. And Haafkens, R. (1979). A Comparison of the Theories to Predict Width and Extent of Vertical, Hydraulically Induced Fractures, Trans., AIME, 101, 8.

Khristianovic, S. A. And Zheltov, Y. P. (1955). Formation of Vertical Fractures by Means of Highly Viscous Liquid, *Proceedings, Fourth Worm Petroleum Congress*, Rome, Italy, pp.579-586.

Nordgren, R. P. (1972). Propagation of a Vertical Hydraulic Fracture, *Society of Petroleum Engineers Journal*, vol. 12, pp. 306-314.

Shen, X. (2012). Cohesive crack for quasi brittle fracture and numerical simulation of hydraulic fracture, *Drilling and Completion in Petroleum Engineering Theory and Numerical Application.*, pp. 175-191.

Simonson, E.R. And Abou-Sayed, A.S. And Clifton, R.J. (1978). Containment of Massive Hydraulic Fractures, *Society of Petroleum Engineers Journal*, 27-32.

Zielonka, M. G. And Searles K. H. (2014). Development and validation of fully-coupled hydraulic fracturing simulation capabilities, *Simulia community conference*.